ACS SYMPOSIUM SERIES 899

Environmental Fate and Safety Management of Agrochemicals

J. Marshall Clark, Editor
University of Massachusetts

Hideo Ohkawa, Editor
Fukuyama University

Sponsored by the
ACS Division of Agrochemicals and
the Pesticide Science Society of Japan

American Chemical Society, Washington, DC

On the basis of the observed products and literatures on the oxidation of phenolic compounds by laccase, the reaction scheme for 8-hydroxybentzon oxidation by laccase is proposed as shown in Fig.5. Initially the phenol moiety of 8-hydroxybentazon is oxidized by laccase and formed phenoxy radicals. Further reactions of these phenoxy radicals are cross coupled with each other and formed dimeric products. Ketone moiety of 8-hydroxybentazon-derived dimers are converted to enol in acidic condition. The coupling reactions most likely occur via C-C coupling at para positions because of their electronic (resonance and inductive) and satiric effects. Proposed reaction pathway leading to the formation of co-polymerization product appears to be initiated by the coupling of two catechol radicals, and subsequent oxidation of that dimmer, resulting in catechol-derived benzoquinone dimer. It appears that a tetrameric copolymerization product is formed by the non-enzymatic addition of two 8-hydroxybentazon to a catechol-derived benzoquinone dimer (Fig. 5).

Reference

1. Kim, J.-E.; Fernandes, E.; Bollag, J.-M. Environ. Sci. Technol. 1997, 31, 2392-2398.

2. Kim, J.-S.; Park, J.-W.; Lee, S.-E.; Kim, J.-E. J. Agric. Food Chem. 2002, 50, 3507-3511.

3. Huber, R.; Otto, S. Rev. Environ. Contam. Toxicol. 1994, 137, 111-134

4. Simmons, K. E.; Minard, R. D.; Bollag, J.-M. Environ. Sci. Technol. 1989, 23, 115-121.

Chapter 10

Predicting Pesticide Volatilization from Bare Soils

Scott R. Yates, Sharon K. Papiernik, and William F. Spencer

U.S. Department of Agriculture, Agricultural Research Service, George E. Brown Jr. Salinity Laboratory, 450 West Big Springs Road, Riverside, CA 92507–4617

Understanding the processes and mechanisms that affect pesticide volatilization from fields is important in developing methods to control emissions. Changes in ambient air temperature and atmospheric stability can strongly affect volatilization. A field study was conducted to measure the volatilization rate. A numerical model was developed to simulate pesticide fate, transport and volatilization. Three volatilization boundary conditions were used to assess the accuracy in predicting the volatilization rates. First, a stagnant boundary layer and isothermal conditions are assumed. Second, a temperature-dependent stagnant boundary layer is considered. A third boundary condition that couples soil and atmospheric processes was found to provide an accurate and realistic simulation of the instantaneous volatilization rates compared to the other boundary conditions. For certain information, such as cumulative emissions, all the boundary conditions yielded similar results and suggest that simpler methods may be useful for this information.

The occurrence of pesticides in the atmosphere or in water supplies is an important national issue (*1-3*). Numerous monitoring studies have demonstrated that agricultural use of pesticides can contribute to both atmospheric and water

contamination. Pesticide movement in the soil zone is affected by many interrelated factors such as the pesticide application methods, soil and environmental conditions, and water management practices. It is expected that with an understanding of pesticide fate and transport, water management and pesticide application practices could be developed that reduce the movement of pesticides outside of the root zone.

Volatilization is an important route of dissipation for pesticides with large vapor pressures or, similarly, large Henry's Law constants (*4-6*). Volatilization has also been shown to be important for pesticides with low to moderate volatility (*7-9*). Volatilization reduces the pesticide available to control pests and reduces the potential of ground water contamination, but increases contamination of the atmosphere. This poses an increased risk to persons living near treated fields, since many pesticides are considered to be carcinogenic (*10*). To protect public health, there is need for more information on the important processes and mechanisms that affect pesticide fate and transport under typical field conditions.

The purpose of this paper was to study the influence of the surface boundary condition on the pattern of pesticide emissions into the atmosphere and to assess the ability to simulate accurate and realistic emission rates. A numerical model was developed to simulate triallate movement in soil, and volatilization into the atmosphere. Three volatilization boundary conditions, with increasing complexity, have been explored: (1) volatilization under isothermal conditions, (2) volatilization in response to solar-driven temperature changes at the soil surface, and (3) volatilization coupled to atmospheric processes.

Methods

The field site was located at the University of California's Moreno Valley Field Station. The soil is a Greenfield sandy loam and is classified as a coarse-loamy-mixed-thermic-typic-Hyploxeralf. The field site was treated with a herbicide, triallate (Fargo 4E; S-(2,3,3-trichloroallyl) diisoproponyl thiocarbamate; CAS: 2303-17-5), by spraying the bare-soil surface with 11.5 kg/ha using 0.1514 m^3 (i.e., 40 gallons) of water. Table 1 gives several properties of triallate. Atmospheric and soil measurements of triallate concentration were collected for a six day period. Atmospheric triallate concentrations were obtained at 10, 30, 51, 80, 120 and 160 cm above the soil surface and represent averages over a two or four hour sampling interval. The four hour sampling intervals occurred during the night-time hours of 2000-2400 and 0000-4000. Meteorological measurements of incoming radiation, net radiation, air temperature, wind speed, wind direction, relative humidity, were obtained for each 10 min interval during this period.

Table 1. Properties of Triallate (*11*)

Molecular Weight	305	$g\ mol^{-1}$
Boiling Point	117	°C
Half life	82	d
Henry's Law Constant, K_H	0.00045	
Organic Carbon Coefficient, K_{oc}	2400	$mL\ g^{-1}$
Saturated Vapor Pressure	$1.1x10^{-4}$	mm Hg
Solubility	4	$mg\ L^{-1}$

Triallate concentration in air was obtained using a series of two polyurethane foam (PUF) plugs held in a glass tube (*12*). A vacuum system was used to draw triallate-laden air into the foam at a prescribed flow rate, 15 L min^{-1}. After each sampling interval, the PUF was stored in a freezer until transport to the laboratory for analysis of the triallate concentration. Soil samples were taken using a coring device 2.5 cm in diameter. Twice each day, a total of 31 samples were collected randomly within the field to a depth of 1 cm.

The triallate in the PUF was removed using soxhlet extraction for 2 h at 60 °C with a azeotropic mixture of hexane and acetone (250 mL total solution). The extracts were concentrated to about 10 mL in a rotary evaporator and analyzed on a gas chromatograph using an electron capture detector. A DB-608 (30m - 0.53mm ID) column with helium as carrier gas was used. The injector and detector temperatures, respectively, were 230 °C and 280 °C. Extracting triallate from the soil samples followed a similar procedure except the extraction time was 8 h. A complete description of the sampling methodology and laboratory analysis is given by Cliath et al. (*13*) and Spencer et al. (*14*).

Model Description

A numerical model was developed to simulate MeBr movement in soil and volatilization into the atmosphere. The model simultaneously solves partial differential equations for nonlinear transport of water, heat, and solute in a variably saturated porous medium. Henry's Law is used to express partitioning between the liquid and gas phases and both liquid and vapor diffusion are included in the simulation. Soil degradation is simulated using a first-order decay reaction and the rate coefficients may differ in each of the three phases (i.e., liquid, solid, or gaseous).

The simulation of saturated-unsaturated water movement in soils is accomplished using the Richard's equation. The simulation of heat movement in soil is obtained using the approach of Sophocleous (*15*) and included diurnal variations in the surface temperature. The governing equation for the fate and transport of triallate is

$$\frac{\partial \theta C}{\partial t} + \frac{\partial \rho_b S}{\partial t} + \frac{\partial \eta G}{\partial t} = \frac{\partial}{\partial z}\left[D_\ell \frac{\partial C}{\partial z} + D_G \frac{\partial G}{\partial z} - qC\right] - \mu_\ell \theta C - \mu_s \rho_b S - \mu_G \eta G \quad (1)$$

where C, S, G are solute concentrations for the liquid, solid, and gaseous phases, respectively (g cm^{-3} or g g^{-1}); q is the volumetric flux density (cm s^{-1}); D_ℓ and D_G are the liquid and vapor phase diffusion coefficients (cm^2 s^{-1}), respectively, μ is a first-order degradation coefficient (s^{-1}) and θ, ρ_b, η, respectively, are the water content (cm^3 cm^{-3}), bulk density (g cm^{-3}) and the air content (cm^3 cm^{-3}). The subscripts: ℓ, s and G indicate liquid, solid, and gaseous phases, respectively. The soil-atmosphere boundary condition is described using

$$-D_E \left.\frac{\partial C}{\partial z}\right|_{z=0} + qC\Big|_{z=0} = -h\left(G - G_{air}\right)\Big|_{z=0} \quad (2)$$

where G_{air} is the concentration in the atmosphere, $D_E = D_\ell + K_H D_G$ is the effective dispersion coefficient and h is the mass transfer coefficient (cm s^{-1}). The mass transfer coefficient is often related to the binary diffusion coefficient (*16*) as

$$h = \frac{D_G^{air}}{b} \quad (3)$$

where b (cm) is the a stagnant boundary layer thickness controlling vapor transport at the soil surface. In Eq. 3, the boundary layer thickness, b, embodies all the processes that affect the transport of chemical across the soil-atmosphere interface.

An alternative formulation for the mass-transfer coefficient that includes atmospheric resistance terms is (*8*).

$$h = \frac{u^*}{7.3\, R_e^{1/4} S_c^{1/2} + \left(\frac{U_r}{u^*} - 5\right)\Phi_m} \quad (4)$$

where R_e and S_c, respectively, are the roughness Reynolds and Schmidt numbers, u^* is the friction velocity (cm s^{-1}), U_r is the wind speed at the measurement height (cm s^{-1}) and Φ_m is an atmospheric stability correction. The denominator of Equation 4, consists of two atmospheric resistance terms, one representing diffusive resistance near the surface and the other aerodynamic resistance from the diffusive layer to the measurement height. To use Eq. 4, many meteorological measurements are needed including gradients of wind speed and temperature.

Three simulations were conducted. Case 1 assumes both D_g^{air} and b in Eq. 3 were constant with D_g^{air} obtained using the average experimental temperature of 9.8 °C. Case 2 assumes b is constant, but D_g^{air} varies according to the ambient temperature as given by the Fuller et al. (*17*) correlation. Case 3 uses Eq. 4 and measured micrometeorological data to evaluate the mass transfer coefficient, h.

Results

Shown in Fig. 1 is a time series of the volatilization rate at the field site during the experimental period. The volatilization rate has a cyclic behavior with peaks occurring predominately during the midday with low values at night. The integer values on the time axis indicate midnight and the vertical dotted lines are at noon. The daily maximum volatilization rate ranged from a high of 59.6 g ha^{-1} h^{-1} on day 1 to a low of 24.2 g ha^{-1} h^{-1} on day 3. The minimum daily volatilization rates were generally less than 5 g ha^{-1} h^{-1}. The low values are primarily due to the effect of the atmospheric stability term (Φ_m in Eq. 4) which tends to suppress the flux during periods of stable conditions ($\Phi_m > 1$, for stable conditions); generally at night. The maximum daily volatilization rates slowly decrease over the course of the experiment, but at a much slower rate than for more volatile compounds such as methyl bromide (*18*). The slow decrease in the volatilization rate is due to a reduction in the concentration gradients at the soil surface as material volatilizes, degrades and diffuses away from the surface.

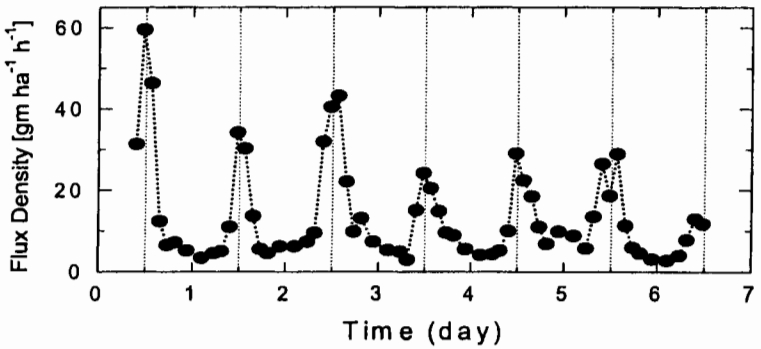

Fig. 1. Volatilization of triallate as a function of time after application.

The relationship between volatilization and atmospheric stability, Φ_m, is clearly shown in Fig. 2, where high volatilization rates generally follow low values of Φ_m, indicating unstable conditions. Low atmospheric concentration occurs during unstable conditions, where buoyancy forces dominate. For stable conditions, mixing in the atmosphere is suppressed causing higher concentrations in the lower atmosphere that reduce gradients at the soil-atmosphere interface. This yields lower volatilization rates compared to unstable conditions.

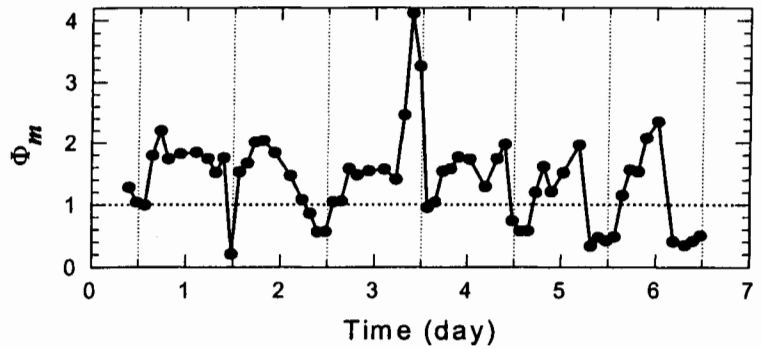

Fig. 2. Stability of the atmosphere as a function of time. Stable atmospheric conditions exist for $\Phi_m > 1$, unstable conditions for $\Phi_m < 1$.

Shown in Fig. 3 is a comparison of simulations for each of the three boundary conditions (i.e., Cases 1-3). The dotted line is the predicted rate of volatilization for Case 1 with a constant boundary layer thickness of 0.5 cm and isothermal

conditions. A nearly constant volatilization rate occurs because the triallate was applied to the soil in a very thin layer and the concentration exceeded the solubility limit. To simulate this, the mass in excess of the solubility limit was partitioned to an immobile phase, that was unavailable for transport. At each time step, if the liquid phase concentration was less than the solubility limit, a portion of the immobile phase was added to the liquid phase to raise the concentration to the solubility limit. This was repeated until the immobile phase was consumed.

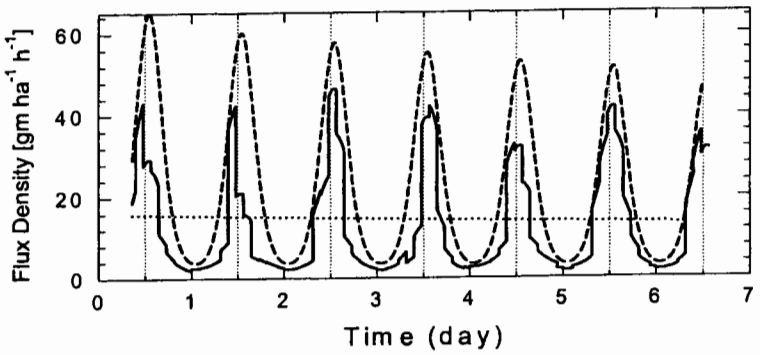

Fig 3. Comparison of predicted volatilization rates from three simulations. The dotted line is Case 1 and assumes the mass transfer coefficient, h, is constant. The dashed line is Case 2 and assumes that h depends on ambient temperature. The solid line is Case 3 and uses Eq. 4 to express h.

Comparing Fig. 1 to the dotted line in Fig. 3 shows a significant disagreement between simulated and measured volatilization rate. This suggests that it is not appropriate to assume isothermal conditions when predicting volatilization rates.

The dashed line in Fig. 3 signifies the predicted volatilization rate for a constant boundary layer thickness and temperature dependent D_g^{air} (i.e., Case 2). Since the air temperature during the experiment varied smoothly, the predicted volatilization rate has a similar behavior. Comparing Case 2 to Fig. 1 shows a general agreement between simulated and measured volatilization rates. This also shows the importance of ambient temperature variations in the simulation.

The solid line in Fig. 3 represents predictions for Case 3. Clearly, the additional micrometeorological information produces a volatilization curve that has commonly-observed erratic variations. This is caused by relatively rapid changes in the wind speed and the stability parameter, Φ_m, and suggests that the effect of ambient temperature and meteorological conditions are important.

Shown in Fig. 4 are measured and predicted cumulative volatilization for the three simulations. Case 1 and Case 3 produce cumulative emission curves that are nearly identical to the measured values. Case 2 produces a curve that deviates from the measurements and has a greater slope. In this instance, it appears to make little difference which approach is used to characterize the surface boundary condition. Even a constant mass transfer coefficient will produce accurate cumulative volatilization provided that the value of h is determined for average experimental conditions.

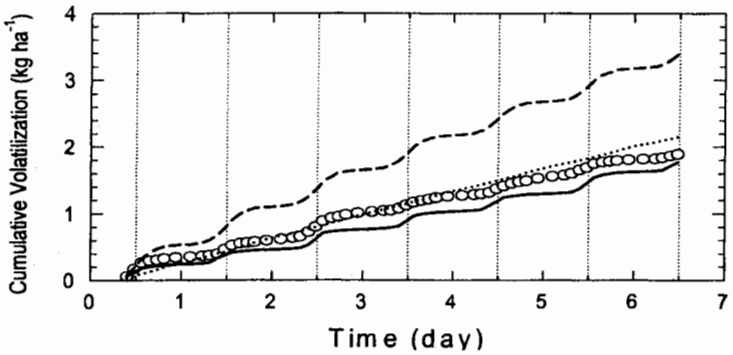

Fig 4. Comparison of cumulative volatilization from three simulations. The dotted line are results from Case 1, the dashed line from Case 2 and the solid line from Case 3. The open circles are measured values.

Figures 3 and 4 can be used to compare the three methods for predicting the volatilization rate, but they do not provide quantitative information that can be used to select the best case, and thereby determine the best choice for characterizing the boundary condition. Shown in Table 2 are three measures of the accuracy of a simulation predicting the measured volatilization rate.

Table 2. Three measures of the accuracy of predicting the volatilization rate.

			SSQ	RMS	Regression		
Method	Area, g ha^{-1}	Area, %	(g ha^{-1} h^{-1})^2	g ha^{-1} h^{-1}	Intercept	Slope	r^2
Measured	1808	100					
Case 1	2096	115.9	8941	94.6	-57.85	4.944	0.079
Case 2	3221	178.2	16841	129.8	0.252	0.531	0.663
Case 3	1642	90.8	5487	74.1	5.048	0.663	0.545

SSQ: sum of squares error; RMS: root-mean square error.

One method for evaluating the accuracy of a simulation is by comparing the total volatilization, obtained by integrating the volatilization rate with time. This is shown in Fig. 4 as a function of time and is reported in Table 2 as areal mass (i.e., g ha^{-1}) and percent relative to the measured volatilization rate. The deviation for Case 1 was approximately 16% and for Case 2 was nearly 80%. Case 3 was the most accurate and was within 10% of the measured values.

Another method for determining accuracy is by comparing the sum of square error (or, equivalently, the root mean square error). For this approach, lower values indicate more accurate predictions. Case 3 had the smallest sum of square error and was nearly 1/3 the magnitude of Case 2.

Regression offers a third method for comparing simulation accuracy. A simulation that fits the measured values perfectly would have a slope, intercept and r^2, respectively, of 1, 0, and 1. Case 3 had a slope that was nearest 1, but Case 2 had an intercept and r^2, respectively, that was closest to 0 and 1. Comparing all three indicators and visual inspection of Figs. 1, 3 and 4 suggest that Case 3 is the most accurate simulation.

Including micrometeorological information into simulations of the volatilization rate should provide more accurate and realistic emissions. This requires considerably more information about atmospheric process, and may be justified when the rate of volatilization is of interest. For the cumulative or total emissions, however, a simulation using micrometeorological data may not be justified because simple boundary conditions were found to be accurate.

Acknowledgments

We acknowledge the assistance of Mark M. Cliath, RoseAnn Lemert, and Christian Taylor in obtaining and analyzing the experimental data.

References

1. United States Department of Agriculture (USDA). 1999. Reducing pesticide risk, Proceedings of the Reducing Pesticide Risk Workshop. USDA, Agricultural Research Service. Washington, DC **1999,** 62 pp.

2. United States Environmental Protection Agency (USEPA). 1987. Agricultural chemicals in ground water: Proposed pesticide strategy. USEPA Office of Pesticides and Toxic Substances. Washington DC **1987,** 150 pp.

3. Kaufmann, C.; Matheson, N. Protecting ground water from agricultural chemicals: Alternative farming strategies for northwest producers. Alternative Energy Resources Organization. Helena, MT. **1990**, 28 pp.
4. Yagi, K.; Williams, J.; Wang, N.Y.; Cicerone, R.J. *Science* **1995**, *267*, 1979-1981.
5. Majewski, M.S.; McChesney, M.M.; Woodrow, J.E.; Pruger, J.H.; Seiber, J.N. *J. Environ. Qual.* **1995**, *24*, 742-752.
6. Yates, S.R., Gan, J., Ernst, F.F., Wang, D. and Yates, M.V. In: *Fumigants: Environmental Fates, Exposure and Analysis*, Am. Chem. Soc. Symp. No. 652, Seiber, J.N. et al., Eds. Washington, DC **1997**, pp. 116-134.
7. Majewski, M.S.; Glotfelty, D.E.; Seiber, J.N. *Atmos. Environ.* **1989**, *23*, 929-938.
8. Baker, J.M.; Koskinen, W.C.; Dowdy, RH. *J. Environ. Qual.* **1996**., *25*, 169-177.
9. Tabernero, M.T.; Alvarez-Benedi, J.; Atienza, J.; Herguedas. A. *Pest Manag. Sci.* **2000**, *56*, 175-180.
10. Doull, J. 1989. American Chemical Society. Washington, DC. 246 pp.
11. Wauchope, R.D.; Buttler, T.M.; Hornsby, A.G.; Augustijn-Beckers, P.W.M.; Burt, J.P. *Rev. Environ. Contamin. Toxic.* **1992**, *123*, 1-155.
12. Turner, B.C.; Glotfelty, D.E. *Anal. Chem.* **1977**, *49*, 7-10.
13. Cliath, M.M.; Spencer, W.F.; Farmer, W.J.; Shoup, T.D.; Grover, R. *J. Agric. Food Chem.* **1980**, *28*, 610-613.
14. Spencer, W.F.; Cliath, M.M.; Jury, W.A.; Zhang, L. *J. Environ. Qual.* **1988**, *17*, 504-509.
15. Sophocleous, M. *Water Resour. Res.* **1979**, *15*, 1195-1206.
16. Jury, W.A.; Spencer, W.F.; Farmer, W.J. *J. Environ. Qual.* **1983**, *12*, 558-564.
17. Fuller, E.N.; Schettler, P.D.; and Giddings, J.C. *Ind. Eng. Chem.* **1966**, *58*, 19-27.
18. Yates, S.R.; Wang, D.; Papiernik, S.K.; Gan, J. *Environmetrics* **2002**, *13*, 569–578.

Environmental Risk Assessment